SUBSPACE-BASED OPTIMIZATION METHOD FOR RECONSTRUCTING PERFECTLY ELECTRIC CONDUCTORS

X. Z. Ye, X. D. Chen, Y. Zhong, and K. Agarwal

National University of Singapore
Singapore 117576, Singapore

Abstract—Reconstruction of perfectly electric conductors (PEC) with transverse magnetic (TM) illumination by a subspace-based optimization method (SOM) is presented. Apart from the information that the unknown object is PEC, no other prior information such as the number of the objects, the approximate locations or the centers is needed. The whole domain is discretized into segments of current lines. Scatterers of arbitrary number and arbitrary shapes are represented by a binary vector, and the descent method is used to solve the discrete optimization problem. Several numerical simulations are chosen to validate the proposed method. In particular, a combination of a line type object and a rectangular shape object is successfully reconstructed. The subspace-based optimization method for PEC scatterers is found to be more complex than its counterpart for dielectric scatterers.

1. INTRODUCTION

Due to its wide application in the field of medical imaging, non-destructive testing and remote sensing, the inverse scattering problem has been of great interest. This paper investigates the inverse scattering problem of reconstructing perfectly electric conductors (PEC), i.e., to reconstruct the locations, contours and the exact number of PEC objects by utilizing the measured scattered field.

The traditional method is to use the so called shape function to represent the contour of the scatterers. Spline function or the Fourier series under local coordinate are most commonly used [1, 2]. This method requires an initial guess of the number and the approximate locations of the scatterers. In situations where such a prior information

---

Corresponding author: X. D. Chen (elechenx@nus.edu.sg).

is not available, the domain of interest is discretized into pixels and consequently PEC objects of arbitrary numbers and shapes can be represented by choosing certain pixels to be PEC [3, 4]. However, aforementioned methods deal with only closed-contour PEC objects, and are not able to reconstruct very thin structures, which are referred to as line-shape structures. In our work, we propose a PEC reconstruction algorithm that is able to reconstruct both closed-contour and line-shape objects, in the absence of a priori information of the number and the approximate locations of the scatterers. The domain of interest is discretized into line elements, and the SOM [5–8] is used to reconstruct the PEC scatterers.

The original contributions of the paper are as follows: Firstly, it extends the application of SOM from dielectric to PEC scatterers. It should be highlighted that this is not a simple extension since the physics and math for these two cases are significantly different. In dielectric case, both scatterers and background can be represented by permittivity, and subsequently, the Lippmann-Schwinger equation can be applied to the whole domain of interest. In comparison, in PEC case, the electric-field-integral-equation (EFIE) is only applicable to the boundary of PEC scatterer that is however unknown in inverse problem. Thus it is much more difficult to apply the SOM in PEC case than in dielectric case. Secondly, to the best of our knowledge, the proposed algorithm is the first one that is able to reconstruct both closed-contour and line-shape objects. Thirdly, the paper presents several numerical results that demonstrate the successful reconstruction of sub-wavelength PEC structures, in the absence of a priori information on the number and the approximate locations of the scatterers.

2. FORWARD PROBLEM

In this paper, we consider an inverse scattering problem in two-dimensional setting with transverse magnetic (TM) time harmonic illuminations. The whole domain is invariant along the z axis. Suppose that the unknown PEC scatterers are located in a given domain $D \subset R^2$. The background medium is free space, and its permittivity and permeability are denoted as ε_0 and μ_0, respectively. There are N_{inc} plane waves given by $\mathbf{E}_p^{inc}(\mathbf{r}) = \hat{z}e^{i\mathbf{k}_p \cdot \mathbf{r}}$, $p = 1, 2, \ldots, N_{inc}$, incident from different angles onto the domain of interest D. $\mathbf{k}_p$ is the wave vector for the pth incidence and the incident electric field vector is parallel to the z axis. For each incident, the scattered field is detected by N_r antennas symmetrically located on a circle with positions $\mathbf{r}'_q$, $q = 1, 2, \ldots, N_r$.

The domain of interest is discretized into small square subunits,

and side edges of square rather than the square itself are used as the elements to represent scatterers, which is a significant difference from the case of dielectric scatterers. After such discretization, the method of moments (MoM) can be used to solve the forward problem [10]. The center of each PEC line-element is located at $\mathbf{r}_j, j = 1, 2, \ldots, N_0$, where N_0 denotes the total number of the PEC line elements. By using the surface equivalence principle, the PEC scatterer can be replaced by the surface current radiating in free space. From the boundary condition, we know that the total field on the surface of the scatterer should be zero, and the field relationship on the surface reads, by the MoM method,

$$E_z^{inc}(\mathbf{r}_m) = -ik\eta \sum_{j=1}^{N_0} J(\mathbf{r}_j) \int_{j\text{-th segment}} \frac{i}{4} H_0^{(1)}(kR_{mj})dt', m = 1, 2, \ldots, N_0,$$
(1)

where k is the free space wave number, η is the impedance of the free space and $H_0^{(1)}$ is the Henkel function of the first kind of order zero, t' is the length parameter along the jth segment. R_{mj} denotes the distance between the mth and jth segments which is given by $R_{mj} = |\mathbf{r}_m - \mathbf{r}_j|$. When $m = j$, the integral is evaluated by the method described in [10]. After the surface current is obtained, the scattered field received by the antennas outside the domain is given by

$$E_z^{sca}(\mathbf{r}'_q) = ik\eta \sum_{j=1}^{N_0} J(\mathbf{r}_j) \int_{j\text{-th segment}} \frac{i}{4} H_0^{(1)}(kR_{qj})dt',$$
(2)

where $R_{qj} = |\mathbf{r}'_q - \mathbf{r}_j|$, $q = 1, 2, \ldots, N_r$.

3. INVERSE PROBLEM BY SOM

For inverse problem, all the PEC boundary elements are unknown so that Eq. (1) cannot be explicitly established. The counterpart of Eq. (1) in dielectric scatterer scenario is referred to as the state equation [5–7]. In PEC scatterer scenario, the absence of an explicit state equation makes it impossible to directly apply the SOM developed for dielectric scatterer scenario.

Although surface currents exist only on the boundary of PEC scatterers, we suppose that there are surface currents on all line elements in domain D such that we can define $\bar{J} = [J(\mathbf{r}_1), J(\mathbf{r}_2), \ldots, J(\mathbf{r}_N)]^T$, where N is the total number of line elements in the domain and the center of each line-element is located at $\mathbf{r}_n, n = 1, 2, \ldots, N$. Note that the entries of $\bar{J}$ equal to zero if the corresponding line elements do not belong to the boundary of PEC.

The total field $\bar{E}^{tot}$, which is also an N-dimensional vector, inside the domain D is given by

$$\bar{E}^{tot} = \bar{E}^{inc} + \bar{\bar{G}}_D \cdot \bar{J} \tag{3}$$

where $\bar{\bar{G}}_D$ denotes the mapping from the induced current to the field inside the domain of interest. For $m, n = 1, 2, \ldots, N$, the entries of $\bar{\bar{G}}_D$ are given by $\bar{\bar{G}}_D(n, m) = -\frac{k\eta}{4} w H_0^{(1)}(k\,|\mathbf{r}_n - \mathbf{r}_m|)$, where $m \neq n$, and $\bar{\bar{G}}_D(n, m) = -\frac{k\eta w}{4}\{1 + i\frac{2}{\pi}[\ln(\frac{\gamma kw}{4}) - 1]\}$ when $m = n$. Here w is the length of the line element and $\gamma = 1.781$ [10]. The scattered field is given by

$$\bar{E}^{sca} = \bar{\bar{G}}_s \cdot \bar{J} \tag{4}$$

where $\bar{E}^{sca} = [E_z^{sca}(\mathbf{r}_1'), E_z^{sca}(\mathbf{r}_2'), \ldots, E_z^{sca}(\mathbf{r}_{N_r}')]^{\mathrm{T}}$ and $\bar{\bar{G}}_s(q, m) = -\frac{k\eta}{4} w H_0^{(1)}(k|\mathbf{r}_q' - \mathbf{r}_m|)$ for $q = 1, 2, \ldots, N_r$ and $m = 1, 2, \ldots, N$, while $\bar{\bar{G}}_s$ is the mapping from the current in D to the scattered field measured at receivers. We refer to Eq. (4) as the field equation.

We define an N-dimensional vector $\bar{P}$, which consists of only 1 and 0, as a judgment of whether the edge belongs to the PEC boundary. In another word, the dimension of vector $\bar{P}$ is equal to the total number of line elements in domain D and a '1' element represents the PEC element and a '0' element represents the free space area. Noticing the fact that $\bar{E}^{tot}$ vanishes on the PEC boundary and in the meanwhile $\bar{J}$ equals to zero for the elements which do not belong to the boundary, we are able to arrive at the following relative residue equation, which is the counterpart of the relative residue in the state equation in the dielectric scatterer scenario [5–7],

$$\Delta^{sta} = \frac{\left\|(\overline{\sim P}) \cdot \bar{J}\right\|^2}{\left\|\bar{J}^s\right\|^2} + \frac{\left\|(\bar{\bar{P}}) \cdot \bar{E}^{tot}\right\|^2}{\left\|\bar{E}^d\right\|^2}, \tag{5}$$

where $\|\cdot\|$ is the Euclidean length of a vector, $\bar{\bar{P}}$ is the diagonal matrix with $\bar{P}$ in the diagonal, and $\overline{\sim P}$ is the diagonal matrix with the complement of $\bar{P}$ in the diagonal. $\bar{J}^s$ is the deterministic part of the induced current which will be introduced later. $\bar{E}^d = \bar{\bar{G}}_D \cdot \bar{J}^s$ is electric field generated by deterministic part of the induced current.

Following the SOM algorithm proposed in [5], the induced current is decomposed into two orthogonally complementary parts: the deterministic part $\bar{J}^s$ and the ambiguous part $\bar{J}^n$. The equation can be expressed as $\bar{J} = \bar{J}^s + \bar{J}^n = \bar{\bar{V}}^s\bar{\alpha}^s + \bar{\bar{V}}^n\bar{\alpha}^n$, where $\bar{\bar{V}}^n$ is the noise subspace composed of the last $M - L$ columns of $\bar{\bar{V}}$, and L is the

number of the total singular values that are above a predefined noise-dependent threshold [5]. After $\bar{J}^s$ is determined from the field equation Eq. (4) by the singular value decomposition (SVD) [5], the residue due to the mismatch of the scattering data can be expressed as

$$\Delta^{fie} = \frac{\left\| \bar{\bar{G}}_s \cdot \bar{V}^n \cdot \bar{\alpha}^n + \bar{\bar{G}}_s . \bar{J}^s - \bar{E}^{sca} \right\|^2}{\left\| \bar{E}^{sca} \right\|^2}. \qquad (6)$$

And we can call it the field residue. The optimal solution of $\bar{\alpha}^n$ in the least square sense is given by

$$\bar{\alpha}^n_{opt} = \bar{\bar{A}}^{-1} \cdot \bar{B} \qquad (7)$$

where $\bar{\bar{A}} = \left\| \bar{E}^d \right\|^2 [(\overline{\sim P}) \cdot \bar{V}^n]^* \cdot [(\overline{\sim P}) \cdot \bar{V}^n] + \left\| \bar{J}^s \right\|^2 (\bar{P} \cdot \bar{\bar{G}}_D \cdot \bar{V}^n)^* \cdot (\bar{P} \cdot \bar{\bar{G}}_D \cdot \bar{V}^n)$, $\bar{B} = -\left\| \bar{E}^d \right\|^2 [(\overline{\sim P} \cdot \bar{V}^n)^* \cdot (\overline{\sim P} \cdot \bar{J}^s)] - \left\| \bar{J}^s \right\|^2 [(\bar{P} \cdot \bar{\bar{G}}_D \cdot \bar{V}^n)^* \cdot [\bar{P} \cdot (\bar{E}^{inc} + \bar{\bar{G}}_D \cdot \bar{J}^s)]$, and the inverse is understood as the pseudoinverse.

The total relative residue is defined to be

$$\Delta^{tot} = \Delta^{fie} + \Delta^{sta} \qquad (8)$$

For each of the incidence $\bar{E}^{inc}_p$, the total relative residue can be calculated as Δ^{tot}_p, $p = 1, 2, \ldots, N_{inc}$. The vector $\bar{P}$ can be obtained by minimizing the following objective function

$$f(\bar{P}) = \sum_{p=1}^{N_{inc}} \Delta^{tot}_p \qquad (9)$$

Since we have already represented $\bar{\alpha}^n$ as the function of $\bar{P}$, there is only one unknown argument $\bar{P}$ left in the optimization equation. The discrete descent optimization method is chosen to minimize the objective function (9). Let the initial guess of $\bar{P}$ as a vector of zeros, i.e., consider all the line elements in the domain as free space. In each iteration, we change each element of $\bar{P}$ into its complement and check whether the objective function decreases, and keep the value which gives smaller residue in the objective function. It is worth mentioning that in the objective function, the relative residue in the state equation can be regarded as some kind of regularization term, and thus no additional regularization method is needed in minimizing (9), as has been done in the previous versions of SOM [5–8].

4. NUMERICAL RESULT

In this section, we give four numerical simulations to validate the algorithm. The domain D is a square with the dimension of $0.6\lambda \times 0.6\lambda$

and is discretized into 15×15 square cells, the centers of which are represented by the vertexes of blue lines. The contour of the PEC is represented in yellow lines while the other line elements are represented by red ones. A total number of $N_{inc} = 10$ incident waves are evenly distributed in $[0, 2\pi)$, with $\mathbf{k}_p = k(\hat{x} \cos \phi_p + \hat{y} \sin \phi_p), p = 1, 2, \ldots, N_{inc}$. $N_r = 30$ receivers are equally distributed on a circle of radius 5λ. The method of moments (MoM) is used to generate the forward scattering data $\bar{E}^{sca}$, which is recorded in the format of the multistatic response (MSR) matrix with the size of $N_r \times N_{inc}$ [9]. Then white Gaussian noise $\bar{\bar{\kappa}}$ is added to the MSR matrix, and the resultant noisy matrix $\bar{\bar{K}} + \bar{\bar{\kappa}}$ is treated as the measured MSR matrix and is used to reconstruct scatterers. The noise level is quantified by the noise-to-signal ratio defined as $\frac{\|\bar{\bar{\kappa}}\|_F}{\|\bar{\bar{K}}\|_F}$, where $\|\cdot\|_F$ denotes the Frobenius norm of a matrix. The initial guess in the optimization problem is free space, i.e. $\bar{P} = 0$. Since the PEC scatterer is impenetrable, it does not change the scattered field whether the internal edges are detected as PEC or air as long as the boundary is correctly detected as PEC. The value of L can be chosen using the criteria presented in [8].

The first numerical example is a circle with radius 0.15λ located in the middle of the region, as shown in Fig. 2(a). Assume the scattered field is obtained without any noise added. The value of L is chosen to be 11, by referring to the spectrum of matrix $\bar{\bar{G}}_s$ as shown in Fig. 1. After 10 iterations, the objective function has fallen to be 3.9499×10^{-23}, and the PEC boundary is reconstructed completely as shown in Fig. 2(b), where the light-blue line with triangle vertex stands for the reconstructed PEC sections of line.

In the second numerical example, two squares of side length 0.14λ are located at $(-0.17\lambda, 0.17\lambda)$ and $(0.17\lambda, -0.17\lambda)$, respectively as shown in Fig. 3(a). For convenience, we refer to the square on the left as number one and the one on the right as number two. The
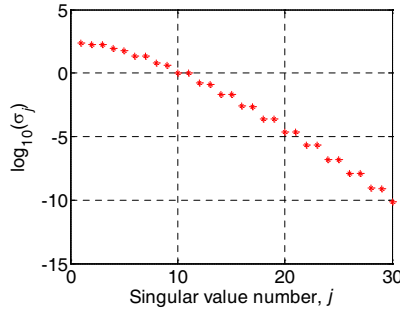
Figure 1. Singular values of the matrix $\bar{\bar{G}}_s$ in all numerical simulations.

separation from the right lower corner of square number one to the left upper corner of square number two is about 0.3λ. 10% white Gaussian noise is added to the exact scattering data. The L chosen here is 4 because of the added noise. After 26 iterations the objective function has been minimized to be 1.8803×10^{-3}, and the corresponding contour of the reconstructed pattern is plotted in Fig. 3(b). It is clearly seen that the region in between the squares are indentified as free space while there are two rectangular-liked shaped PEC scatterers located around $(-0.17\lambda, 0.17\lambda)$ and $(0.17\lambda, -0.17\lambda)$. The sizes of the reconstructed scatterers are almost the same as the original ones. The result is satisfactory, considering the close distance of scatterers and the presence of 10% noise.
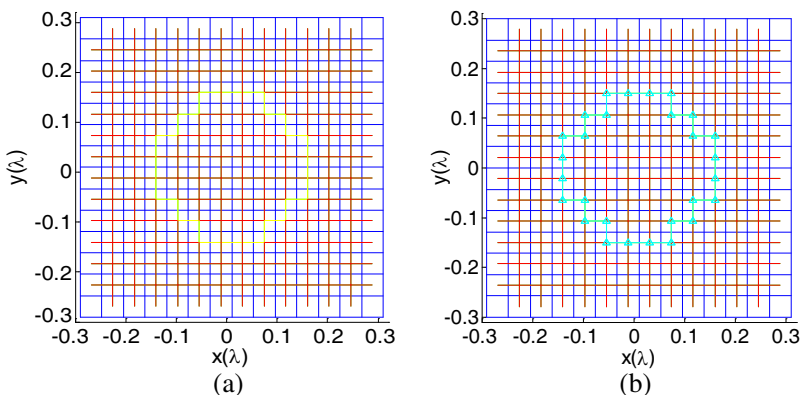
Figure 2. A circle with radius 0.15λ. (a) Exact contour. (b) Reconstructed contour.
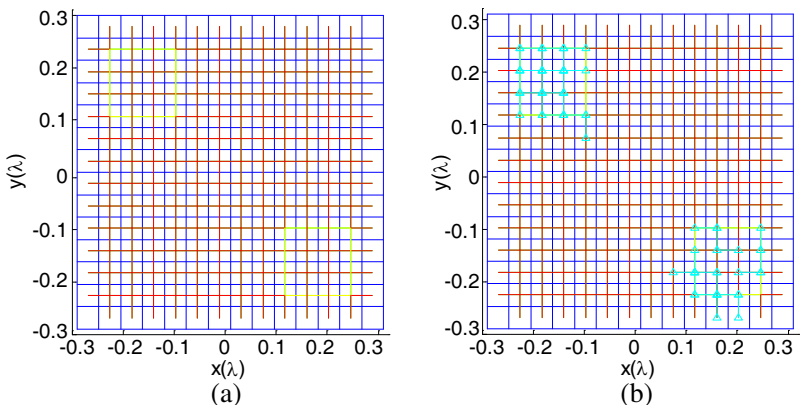
Figure 3. Two squares separated by 0.3λ. (a) Exact contour. (b) Reconstructed contour under 10% white Gaussian noise.

In the third example we deal with a line-shape scatterer, which resembles an "L" (Fig. 4(a)). In presence of 5% noise, we successfully reconstructed the single line with only one segment missing after 16 iterations. And the L chosen here equals to 6 with the objective function minimized to be 6.4665×10^{-4}.

In the last example, we test the proposed method for reconstructing a combination of a closed-contour scatterer and a line-shape scatterer. A rectangular and a straight line PEC scatterer are located in the domain as shown in Fig. 5(a). 10% white Gaussian noise is added and L is chosen to be 4 which is the same as in the second
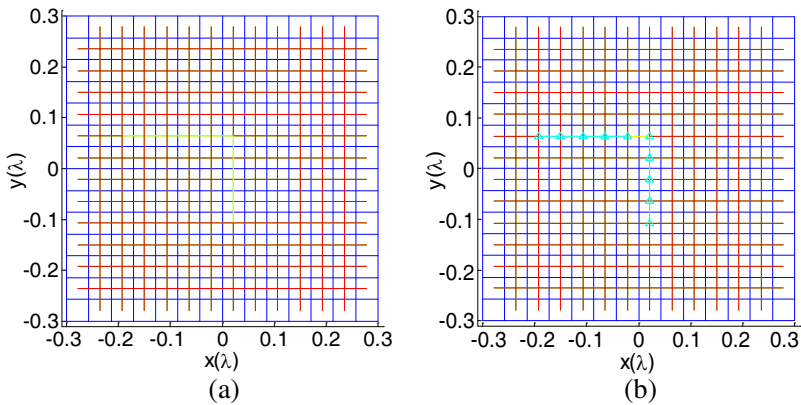
Figure 4. Single line shaped scatterer. (a) Exact contour. (b) Reconstructed contour under 5% white Gaussian noise.
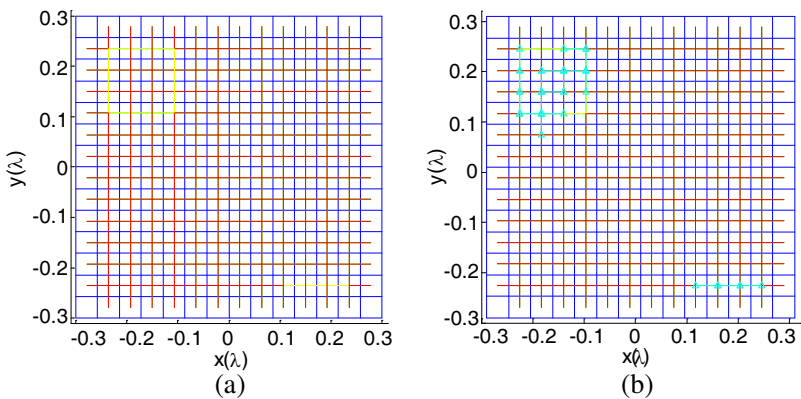
Figure 5. A combination of a square and a single straight line. (a) Exact contour. (b) Reconstructed contour under 10% white Gaussian noise.

example. After 54 iterations, the objective function is minimized to 1.6917×10^{-3} and from the reconstructed figure we can clearly see that there is a single line and a rectangular shaped scatterer located in the domain with an obvious gap.

5. DISCUSSION AND CONCLUSION

The paper extends the application of SOM from dielectric to PEC scatterers. The advantages of SOM that have been presented in dielectric case [5–8] are also exhibited in the PEC case, such as fast convergence and robustness against noise. The essences of SOM, no matter in dielectric or PEC cases, lie in decomposing the induced current into deterministic and ambiguous part. Whereas the deterministic part is obtained by SVD without resourcing to optimization, the ambiguous part is obtained by solving an optimization problem in which the searching dimension is smaller than that of the original problem. However, since these two cases are significantly different in both physics and math, the SOM in PEC case is consequently much different from the SOM in dielectric case. The following aspects are worth discussing.

1. In the PEC case, the boundary of PEC scatterers are to be reconstructed, and subsequently, the line-element is used as the basic element to represent scatterers of arbitrary numbers and shapes, including a combination of closed-contour and line-shape scatterers that to the best of our knowledge has never been explored so far. This is significantly different from the dielectric case where the square-element is used as the basic element.

2. In PEC case, induced currents are surface currents and the condition that tangential electric field vanishes at the surface leads to the EFIE. However, in inverse problems, the boundary of PEC is unknown so that the EFIE cannot be applied to the whole domain of interest. We highlight that for this reason, the objective function of SOM in PEC case is much more difficult to build up than that in dielectric case [11]. Proposing the model of the relative state residue is one of the main contributions of the paper.

3. In PEC case, the shape function P is binary, and the optimization problem is a discrete one. This is different from the dielectric case which is a continuous optimization problem. The optimization method used in this paper is the discrete descent method. In the future research work, we will adopt genetic algorithm (GA) which is more suitable for binary optimization problem.

REFERENCES

1. Chiu, C. and P. Liu, "Image reconstruction of a perfectly conducting cylinder by the genetic algorithm," *IEEE Proc. — Microw. Antennas Propag.*, Vol. 143, 249–253, 1996.

2. Qing, A., "Electromagnetic inverse scattering of multiple two-dimensional perfectly conducting objects by the differential evolution strategy," *IEEE Transactions on Antennas and Propagation*, Vol. 51, 1251–1262, 2003.

3. Takenaka, T., Z. Meng, T. Tanaka, and W. Chew, "Local shape function combined with genetic algorithm applied to inverse scattering for strips," *Microwave and Optical Technology Letters*, Vol. 16, 337–341, 1997.

4. Meng, Z. Q., T. Takenaka, and T. Tanaka, "Image reconstruction of two-dimensional impenetrable objects using genetic algorithm," *Journal of Electromagnetic Waves and Applications*, Vol. 13, No. 1, 95–118, 1999.

5. Chen, X., "Application of signal-subspace and optimization methods in reconstructing extended scatterers," *J. Opt. Soc. Am.*, Vol. 26, 1022–1026, 2009.

6. Zhong, Y. and X. Chen, "Twofold subspace-based optimization method for solving inverse scattering problems," *Inverse Problems*, Vol. 28, 085003, 2009.

7. Chen, X., "Subspace-based optimization method for solving inverse scattering problems," *IEEE Trans. Geosci. Remote Sens.*, accepted, 2009.

8. Chen, X. D., "Subspace-based optimization method in electric impedance tomography," *Journal of Electromagnetic Waves and Applications*, Vol. 23, No. 11–12, 1397–1406, 2009.

9. Chen, X., "Time-reversal operator for a small sphere in electromagnetic fields," *Journal of Electromagnetic Waves and Applications*, Vol. 21, No. 9, 1219–1230, 2007.

10. Peterson, A. F., S. L. Ray, and R. Mittra, *Computational Methods for Electromagnetics*, IEEE Press, New York, 1998.

11. Chew, W. and Y. Wang, "Reconstruction of two-dimensional permittivity distribution using the distorted born iterative method," *IEEE Trans. Med. Imaging*, Vol. 9, 218–225, 1990.